Towards an accurate radar waveform recognition algorithm based on dense CNN

Weijian Si[1] · **Chenxia Wan**[1] · **Chunjie Zhang**[1]

© Springer Science+Business Media, LLC, part of Springer Nature 2020

Abstract

Existing algorithms for radar waveform classification currently exhibit the lower recognition accuracy, especially at the lower signal to noise ratio (SNR) environment. To remedy these flaws, this paper proposes an accurate automatic modulation classification algorithm based on dense convolutional neural networks (AAMC-DCNN). The algorithm owns the competitive advantages of strengthening the feature reuse and extracting the detailed feature, for improving the recognition performance of radar waveform at the lower SNR. First, the dense convolutional neural networks (CNN) are designed, which connects each layer to every other layer in a feed-forward pattern. In the latter, 8 types of signals are converted into time-frequency images by choi-williams distribution (CWD), and the large training and testing datasets are fabricated. Then, the transfer learning and Adam optimization are introduced. Finally, the experimental analyses are carried out to evaluate the recognition performance. It is worth mentioning that the classification accuracy can be up to 93.4% when the SNR is −8 dB, and even reach to 100% at 0 dB, which demonstrates the superior performance over others. The present work provides a sound experimental basis for further studying automatic modulation classification for the sake of future field application in electronic warfare systems.

1 Introduction

Automatic radar waveform recognition technology can be capable of identifying the low probability of intercept (LPI) radar waveform of received signal, which plays an essential role

✉ Chunjie Zhang
   zhangchunjie@hrbeu.edu.cn

[1]   College of Information and Communication Engineering, Harbin Engineering University, Harbin 150001, China

in electronic warfare systems, such as electronic support, electronic intelligence, electronic attack, and so on [1, 13]. With the remarkable development of radar technology and the working environment of radar at the lower SNR in the recent decades, the modulation types of LPI radar signal have become more and more complicated and diversified [24]. Therefore, it is crucial to explore a more accurate approach to recognize the radar waveform at the lower SNR environment.

Some LPI waveform automatic recognition techniques have been proposed in recent years [2], which utilized feature extraction and classification techniques to extract features from the LPI radar signal and classify the types of signal, respectively. For the feature extraction, time-frequency conversion technology can transform the signal waveform into time-frequency images (TFI), such as wigner ville distribution (WVD) [11, 28] and choi-willian distribution (CWD) [15, 35]. In addition, a combination of two time-frequency conversions has also been researched, for example, smooth pseudo wigner-ville distribution (SPWVD) and born-jordan distribution (BJD) [38], WVD and CWD [20, 36]. Moreover, with the significant achievement of artificial intelligence, deep learning has aroused widespread concern and widely applied in various fields, for its excellent feature extraction and classification capabilities [39]. VGG [25], Highway Networks [26], Residual Networks (ResNets) [7], and DenseNets [8] have been proposed. Dense connection as well as residual connections have been widely used in computer vision tasks, such as object tracking [18] and video object segmentation [19, 29].

The advanced network model, including the recurrent neural networks (RNN) [16], deep belief networks (DBN) [4], support vector machine (SVM) [6], and convolutional neural networks (CNN) [3, 9, 22, 30, 41], have been proposed for improving the recognition performance of radar waveform. Zhang et al. [37] explored a novel blind modulation classification method based on the time-frequency distribution and CNN. Kong et al. [14] proposed LPI radar waveform recognition technique based on CNN and designed the hyperparameters. Wang et al. [31] investigated an automatic modulation classification algorithm based on a joint feature map for discriminating the radar emitter signal, and the overall recognition rate of the six LPI radar signals was up to 97% at SNR of 6 dB. Wan et al. [27] researched an automatic identification system for detecting, tracking and locating low probability radar waveform, and the experimental results showed that the overall recognition rate of the system reached to 94.42% when the SNR was −4 dB. Ma et al. [21] proposed an autocorrelation feature image construction technique (ACFICT) combined with CNN, and the simulation results showed that when the SNR was −6 dB, the overall recognition rate of the method was up to 88%. Wang et al. [32] proposed a novel waveform recognition method based on an adversarial unsupervised domain adaptation, which incorporated adversarial learning to improve the cross-scenario recognition performance. Zhu et al. [40] proposed a deep multi-label based multiuser automatic modulation classification framework (MLAMC) for compound signals, which validated the effectiveness and superiority of the method. Wei et al. [33] proposed a novel network that combined a shallow CNN, long short-term memory (LSTM) network and deep neural network (DNN) for recognizing six types of radar signals, which demonstrated that the accuracies in autocorrelation domain were all more than 90%.

A common limitation of the above-mentioned work is that the recognition accuracy is still low up to now, especially at the lower SNR environment, and the recognition types of the radar waveform are relatively less. To remedy these flaws, an accurate automatic modulation classification algorithm based on dense convolutional neural networks (AAMC-DCNN) is

proposed. The algorithm owns the competitive advantages of strengthening the feature reuse and extracting the detailed feature, for improving the recognition performance of radar waveform at the lower SNR. The proposed AAMC-DCNN mainly consists of data pre-processing, feature extraction and classification. In the first part, the eight types of signal are converted into time-frequency images by choi-williams distribution (CWD), and the large training and testing datasets are fabricated. In the second part, the dense convolutional neural networks (CNN) are designed, and the transfer learning and Adam optimization are introduced. Finally, the experimental analyses are carried out to evaluate the recognition performance. It is worth mentioning that the classification accuracy can be up to 93.4% when the SNR is −8 dB, and even reach to 100% at 0 dB.

This paper is organized as follows. The overall structure of the LPI radar waveform recognition algorithm is proposed in Section 2. Signal model and basic theory of time-frequency distribution are introduced in Section 3. A dense CNN model for LPI radar waveform recognition algorithm is designed in Section 4. The large dataset is fabricated, and the recognition performance of the proposed method is fully investigated by experiment in Section 5. Conclusion of this work is drawn in Section 6.

2 Designing of AAMC-DCNN

Figure 1 illustrates the proposed AAMC-DCNN. The algorithm aims to improve radar waveform recognition accuracy and enhance robustness, especially at the lower SNR environment, which mainly consists of data pre-processing, dense CNN feature extraction and radar waveform classification.

As can be known from Fig. 1 that LPI radar waveform signal will transform 2-D TFI by using choi-williams distribution (CWD) transformation in the first part. The dataset can be obtained by transforming and binarizing the TFI. The partial pre-processed dataset, about 70%, is selected as the training. While, the remained dataset is used as the testing. In the second part, the dense CNN is proposed for the sake of feature extraction and classification, which owns the competitive advantage of improving the recognition performance of radar waveform at the lower SNR by strengthening the feature reuse and extracting the detailed feature. It is attributed to the fact that it possesses a dense connection mechanism. In order to accelerate and optimize the learning efficiency of the proposed model that without learning from scratch as before, the transfer learning and Adam optimization are employed to share the learned parameters with the proposed model. The dense CNN is first pre-training by using ImageNet, and the obtained pre-training parameters are saved. Then, the fabricated training dataset is input into the designed dense CNN model to extract radar waveform feature by means of using the pre-training parameters, and the Adam optimization is used to optimize and train the network parameters. The testing dataset is eventually sent into SoftMax classifier, and the eight types of LPI radar waveform classification results can be obtained accurately.
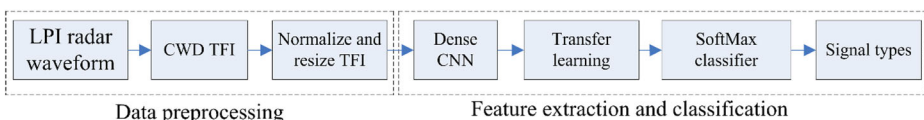
Fig. 1 AAMC-DCNN framework

3 Data pre-processing

The CWD time-frequency analysis is utilized to convert the LPI radar waveform into the 2-D TFI, which can be binarized and then transformed into the suitable size to send into the dense CNN.

3.1 Signal model

This paper pays close attention to the common LPI radar signals, including binary frequency shift keying (2FSK), 4-frequency shift keying (4FSK), binary phase shift keying (BPSK), even quadratic frequency modulation (EQFM), Frank, linear frequency modulation (LFM), normal signal (NS), and sinusoidal frequency modulation (SFM), which can be processed by the gaussian white noise (GWN). The SNR is used to add the recognition complexity, and can be written as $SNR = 10\log_{10}\left(\sigma_s^2\right)/\sigma_\varepsilon^2$, where σ_s^2 and σ_ε^2 represent the variances of signal and noise, respectively. The LPI radar signal is formulated as [34].

$$z(nT) = s(nT) + m(nT) \tag{1}$$

where $z(nT)$ refers to the received LPI radar waveform signal; $s(nT)$ represents n-th sampling signal of period T; $m(nT)$ is the n-th GWN sample of power σ_ε^2.

3.2 Time-frequency distribution

The CWD refers to a Cohen-type time-frequency distribution [17]. It not only expresses the detected signals in detail by introducing a kernel function, but also prevents significantly the cross terms. The $C(t,\omega)$ refers to the obtained result of CWD time-frequency conversion, which is given as

$$C(t,\omega) = \iiint_\infty e^{j2\pi\xi(s-t)} f(\xi,\tau) \cdot x(s+t/2) \cdot x^*(s-t/2) \cdot e^{-j\omega\tau} d\xi ds d\tau \tag{2}$$

where $f(\xi,\tau)$ is a kernel function, referring to a 2-D low-pass filter, which is defined as

$$f(\xi,\tau) = e^{(\pi\xi\tau)^2/2\sigma} \tag{3}$$

where σ represents the controllable factor, and it decides the bandwidth of the filter. σ is set to 1 for balancing the cross terms and resolution in TFI of radar waveform. The obtained CWD transformation results of the eight types of LPI radar signal are shown in Fig. 2.

4 Feature extraction and classification

Inspired by Huang et al. [8], a dense CNN is proposed for extracting feature and classifying the LPI radar signals. In order to speed up and optimize the learning efficiency of the proposed model that without learning from scratch as before, the transfer learning [23] is also introduced in this model. The Adam optimization algorithm [12] is adopted to optimize the proposed dense CNN parameters. The specific steps of the implementation approach are as follows.
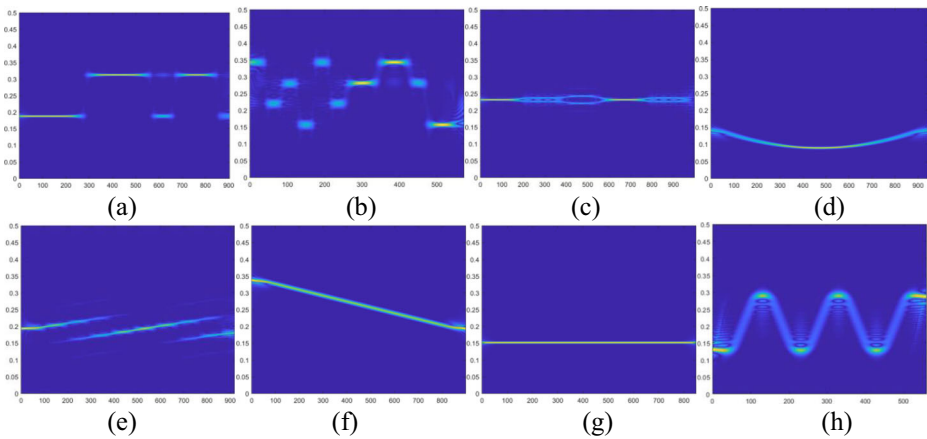
Fig. 2 CWD transformation results of the eight types of LPI radar signal: (**a**) 2FSK; (**b**) 4FSK; (**c**) BPSK; (**d**) EQFM; (**e**) Frank; (**f**) LFM; (**g**) NS; (**h**) SFM

4.1 Dense CNN

Figure 3 illustrates the proposed dense CNN model for extracting feature maps of radar waveform and classifying the types of radar signal. The model possesses the competitive advantages of improving the recognition performance of radar waveform at the lower SNR by alleviating the vanishing-gradient problem, strengthening the feature propagation, encouraging the feature reuse, extracting the detailed feature, and substantially reducing the parameters.

It can be known from Fig. 3 that the proposed dense CNN model includes five dense blocks (naming dense-1, dense-2, dense-3, dense-4, and dense-5) and four transition layers (naming transition-1, transition-2, transition-3, and transition-4). The training dataset is first input into the convolutional layer with the kernel size of 7×7 for feature extraction. The extracted features are input into the max pooling layer with the kernel size of 3×3, for reducing the dimension of the feature maps. They are then sent into the dense-1, including 6 convolutional layers with the kernel sizes of 1×1 and 3×3, respectively, aiming to further extract feature. The decreased input feature maps not only can improve the computation efficiency, but also integrate the features of each channel. The obtained feature maps are feed into the transition-1, consisting of a batch normalization, a convolutional layer with a kernel size of 1×1 and an
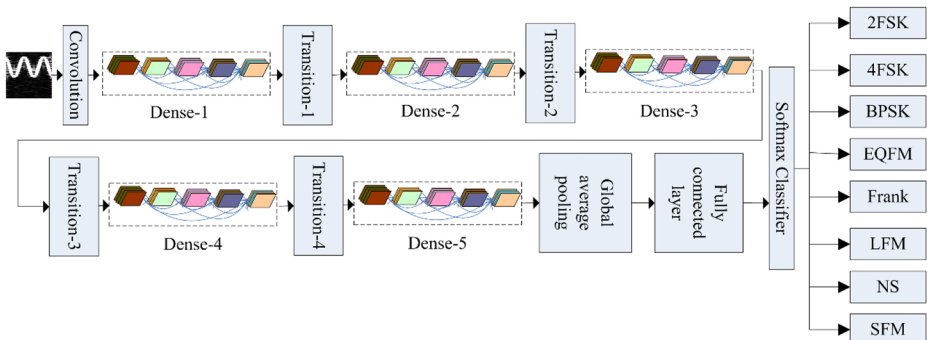
Fig. 3 Modified dense CNN model framework

average pooling layer with the kernel size of 2×2, for matching the size of the feature maps. It has an ability of taking full advantage of the learned feature maps and decreasing unnecessary external noise without using zero padding. The action mechanisms of the following dense blocks and transition layers are similar to the dense-1 and transition-1, respectively. The eventual feature maps extracting from dense-5 are input into the classification layer, which include a global average pooling layer with a filter size of 7×7, an 8-D full connection layer, and a SoftMax classifier. The detailed parameters of the proposed dense CNN are shown in Table 1.

The dense CNN owns a more radical dense-connection mechanism compared with DenseNet [8], which interconnects all the layers. Figure 4 shows the connection mechanism of a dense block.

It is observed from Fig. 4 that each layer is connected to all previous layers on the channel dimension and serves as the input to the next layer. For the l-th layer network, the dense block consists of $l(l + 1)/2$ connections. In addition, the dense block is also defined as the feature map of directly contacting with different layers, which can reuse feature and thus improve efficiency. The l-th layer can receive the feature maps of all preceding layers, which can be given as

$$y_l = H_l([y_0, y_1, \cdots, y_{l-1}]) \tag{4}$$

where $H_l(\cdot)$ refers to non-linear transformation function, including a series of batch normalization [10], rectified linear units (ReLU) [5], pooling and convolution layer. $[y_0, y_1, \cdots, y_{l-1}]$ represents the concatenation of the feature maps produced in layers 0, 1,…, l-1, respectively.

To maintain consistent feature map sizes in the dense CNN connection, the dense block and transition structure are utilized in this model. The transition module can connect two adjacent dense blocks and reduce the size of the feature maps by means of average pooling layer. The m

Table 1 Parameters of the dense CNN

| Layers	Size	Filters	Stride	Output	Padding
Convolution	7×7	1	2	224×224	3
Max pooling	3×3		2	112×112	
Dense-1	1×1 convolution	6	1	112×112	1
	3×3 convolution	6	1	112×112	1
Transition-1	1×1 convolution	1	1	112×112	1
	2×2 average pooling		2	56×56	
Dense-2	1×1 convolution	12	1	56×56	1
	3×3 convolution	12	1	56×56	1
Transition-2	1×1 convolution	1	1	56×56	1
	2×2 average pooling		2	28×28	
Dense-3	1×1 convolution	48	1	28×28	1
	3×3 convolution	48	1	28×28	1
Transition-3	1×1 convolution	1	1	28×28	1
	2×2 average pooling		2	14×14	
Dense-4	1×1 convolution	32	1	14×14	1
	3×3 convolution	32	1	14×14	1
Transition-4	1×1 convolution	1	1	14×14	1
	2×2 average pooling		2	7×7	
Dense-5	1×1 convolution	32	1	7×7	1
	3×3 convolution	32	1	7×7	1
Classification layer	7×7 global average pooling	–	–	1×1	–
	8-D fully connected layer				
	SoftMax				
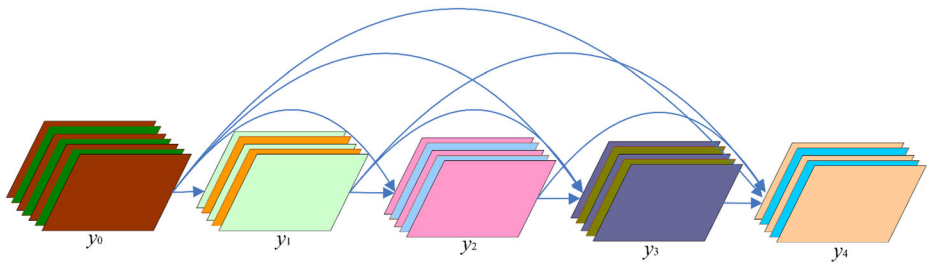
Fig. 4 Dense block

feature map channels obtained by dense block are input into the transition layer, and it can produce $\theta * m$ feature maps, where θ is the compression rate. θ is set to 0.5 in this paper for reducing network parameters. Therefore, the transition layer can act as a compression model to some extent.

4.2 Pre-training and optimization

One of the most powerful ideas in deep learning is transfer learning, in which neural networks can acquire knowledge from one task sometimes and apply successfully that knowledge to another similar task. The introduction of transfer learning could reduce the training time of the network model and eliminate the need to start from scratch on a new dataset to some extent. In this paper, the proposed dense CNN is pre-training on the ImageNet dataset, and the pre-trained parameters are saved to later train the LPI radar signal dataset in the dense CNN model.

Adam is considered as a first-order optimization algorithm that can replace the traditional stochastic gradient descent process, which owns the powerful advantages of decreasing the computation resource and speeding up the model convergence [12]. It can update the weight of neural network iteratively based on the training data, and an important feature of its updating rules is to choose the step size carefully. Assuming ε equal to 0, the effective descent step size of the time step t and parameter space can be written as

$$\Delta_t = \frac{\alpha \cdot \widehat{m}_t}{\sqrt{\widehat{v}_t}} \tag{5}$$

where α represents the step parameter; m_t refers to the exponential moving averages of the gradient; v_t is the squared gradient; $\widehat{m}_t$ is the bias-corrected estimate of m_t; $\widehat{v}_t$ is the estimate of v_t.

The approximation magnitude of the effective step size of each time in the parameter space is limited by the step size factor α, which is given as

$$|\Delta_t| \stackrel{<}{\approx} \alpha \cdot \frac{1-\beta_1}{\sqrt{1-\beta_2}} \tag{6}$$

where β_1 and β_2 are the hyper-parameters, which control the exponential decay rates of these moving averages.

The initialization bias is used to correct the term for Adam algorithm, which will be derived from the second-order moment estimation. The gradient of the stochastic objective function f can be first obtained, and then its second-order original moment is estimated by using the

exponential moving mean and decay rate β_2 of the squared gradient. The gradients in time step sequence is defined as $g_1, \ldots, g_T$, respectively, which all obeys the potential gradient distribution g_t, where $g_t \sim p(g_t)$. The exponential moving initialized mean v_0 is equal to zero vector. The updated exponential moving mean at time step t is given as

$$v_t = \beta_2 \cdot v_{t-1} + (1-\beta_2) \cdot g_t^2 \tag{7}$$

where g_t^2 represents the Hadamard product $g_t \odot g_t$. When v is eliminated, it can be rewritten as a function that only contains the gradient and the decay rate on all previous time steps. The Equation is given as

$$v_t = (1-\beta_2) \cdot \sum_{i=1}^{t} \beta_2^{t-i} g_t^2 \tag{8}$$

The expectation operation is conducted for Eq. (8), and the obtained results can be written as

$$\mathrm{E}[v_t] = \mathrm{E}\left[(1-\beta_2) \cdot \sum_{i=1}^{t} \beta_2^{t-i} g_t^2\right] = \mathrm{E}\left[g_t^2\right] \cdot (1-\beta_2) \cdot \sum_{i=1}^{t} \beta_2^{t-i} + \zeta = \mathrm{E}\left[g_t^2\right] \cdot \left(1-\beta_2^t\right) + \zeta \tag{9}$$

If the real second order moment $\mathrm{E}[g_{2i}]$ is stationary, then the ζ is set to 0, otherwise ζ could keep a very small value. It is because the hyper-parameter β_1 can make the moving average distribution of the small weight into gradient. Therefore, the term $\left(1-\beta_2^t\right)$ is only remained by initializing the zero vector.

4.3 Dataset

The radar signal datasets utilized in this paper, consisting of 2FSK, 4FSK, BPSK, EQFM, Frank, LFM, NS, and SFM, are formulated. Table 2 lists the employed radar signal parameters. The frequency parameters of the signals are processed by normalization. In order to analyze the generalization performance of the approach, the parameters of all simulation signals have a dynamic characteristic. The signal length is randomly changed from 512 to 1024.

For the training dataset, there are 1000 samples randomly generated for each signal type at the same SNR condition, and the SNR ranges from −8 to 14 dB at intervals of 2 dB in this paper. Therefore, the obtained training dataset is totally up to 96,000 samples. While, for the testing dataset, 400 samples can be randomly produced for each signal at the same SNR. Therefore, the testing dataset includes 38,400 samples. The training dataset will be used to train the network parameters, while the testing dataset will be utilized to evaluate the recognition performance of radar waveform.

5 Experimental results and analyses

The experimental analyses are conducted to evaluate the performance of the proposed AAMC-DCNN model for recognizing the radar waveform. The network parameters of LPI radar signals and the datasets are first designed. Next, the average recognition accuracy of eight radar signal types of the model is fully verified by the experiment, and performance analyses are carried out to compare with time-frequency feature map using CNN (TFFM-CNN) [28] and joint feature map and CNN (JFM-CNN) [30]. Then, to show the recognition performance of the proposed method at the lower SNR in detail, the confusion matrices are investigated for

Table 2 The parameters of LPI radar signal

Types	Parameter	Range
2FSK	Carrier frequency f_1, f_2	0.01 to 0.46
	Bandwidth Δf	N/32 to N/8
4FSK	f_1 to f_4	0.1 to 0.4
	T_s	N/32 to N/8
BPSK	Barker codes	[11, 25, 35, 38]
	f_0	0.1 to 0.4
	T_s	N/32 to N/16
EQFM	Carrier frequency f_1, f_2	0.05 to 0.4
	Bandwidth Δf	0.05 to 0.3
Frank	f_0	0.1 to 0.4
	T_s	N/100 to N/50
	Phase number M	[4,5,6,7]
LFM	Initial frequency f_c	0.01 to 0.45
	Bandwidth f	0.05 to 0.4
NS	Carrier Frequency f_0	0.1 to 0.4
SFM	Carrier Frequency f_0	0.05 to 0.15
	Bandwidth Δf	0.05 to 0.35

the SNR changes from -8 to -2 dB. Finally, the variation of performance with SNR at a specific modulation type is clearly obtained, and the variation of classification accuracy with SNR for the AAMC-DCNN and JFM-CNN at 2FSK, 4FSK, BPSK and LFM is explored for the comparative analyses. To demonstrate the recognition performance of the proposed AAMC-DCNN over the two another method: TFFM-CNN and JFM-CNN, the average recognition accuracy of the AAMC-DCNN is compared with JFM-CNN and TFFM-CNN for various radar signal types. Figure 5 illustrates the average recognition accuracies of radar signal types of AAMC-DCNN, JFM-CNN and TFFM-CNN with the SNR.

It should be noted that the variable SNR utilized in TFFM-CNN and JFM-CNN is ranged from −4 to 14 dB and 6 to 14 dB, respectively, for comparative analyses. As can be known
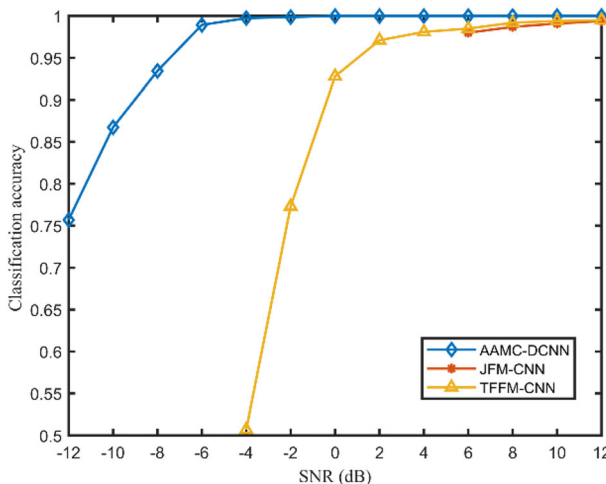
Fig. 5 Variation of average classification accuracy with SNR for AAMC-DCNN, JFM-CNN and TFFM-CNN

from Fig. 5 that the classification accuracy all enhanced with the increase of SNR for these methods, and the recognition accuracy could all reach to 95% when the SNR is larger than 2 dB. When the SNR is at 6 dB, the obtained classification accuracy ratios for AAMC-DCNN, JFM-CNN and TFFM-CNN are 100%, 98%, and 98.5%, respectively. In addition, the proposed AAMC-DCNN demonstrates the superior recognition accuracy over others, especially at lower SNR. The proposed algorithm can be up to 100% at 0 dB. Therefore, the proposed AAMC-DCNN shows an outstanding average classification accuracy for eight signal types. This is attributed to the fact that the proposed dense CNN owns a denser linkage mechanism and can extract more detailed feature.

Furthermore, to more detail show the recognition performance of the proposed AAMC-DCNN at the lower SNR, the confusion matrices are investigated for the SNR changing from −8 to −2 dB. Figure 6 illustrates the confusion matrices of the proposed algorithm at various SNR.
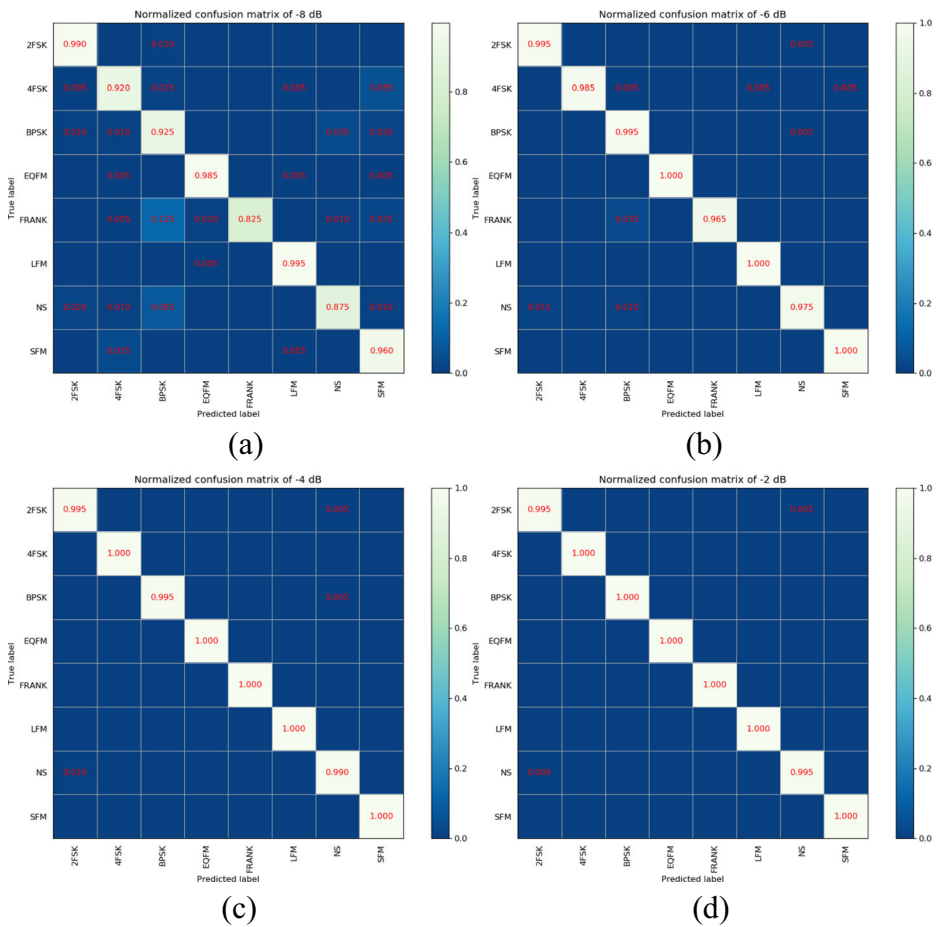

Fig. 6 Confusion matrices of the AAMC-DCNN for the SNR changing from −8 to −2 dB: (**a**) -8 dB; (**b**) -6 dB; (**c**) -4 dB; (**d**) -2 dB

As illustrated from Fig. 6, it is apparent that the classification accuracy of LFM and SFM demonstrates the best performance, while, the error of NS, Frank, and 4FSK are higher than other modulation types. The main discrepancy is due to the fact that Frank and BPSK are easily confused with each other. This can be explained by the dataset that their TFI are similar to each other, as shown in Fig. 2.

To clearly obtain the variation of classification performance with SNR at a specific modulation type, Fig. 7 illustrates the variation of classification accuracy of the proposed AAMC-DCNN and JFM-CNN with SNR at 2FSK, 4FSK, BPSK and LFM.

As can be shown from Fig. 7 that the classification accuracy of the proposed AAMC-DCNN is more than 96% for all signals, and some of them even achieve 100% when the SNR is larger than 0 dB. In addition, the recognition performance of AAMC-DCNN is obviously better than JFM-CNN at the lower SNR. Therefore, the proposed algorithm shows a robust classification ability for various signal types, especially at the lower SNR. The powerful feature extraction and classification capability of the proposed dense CNN model are important reasons for explaining the excellent classification performance.
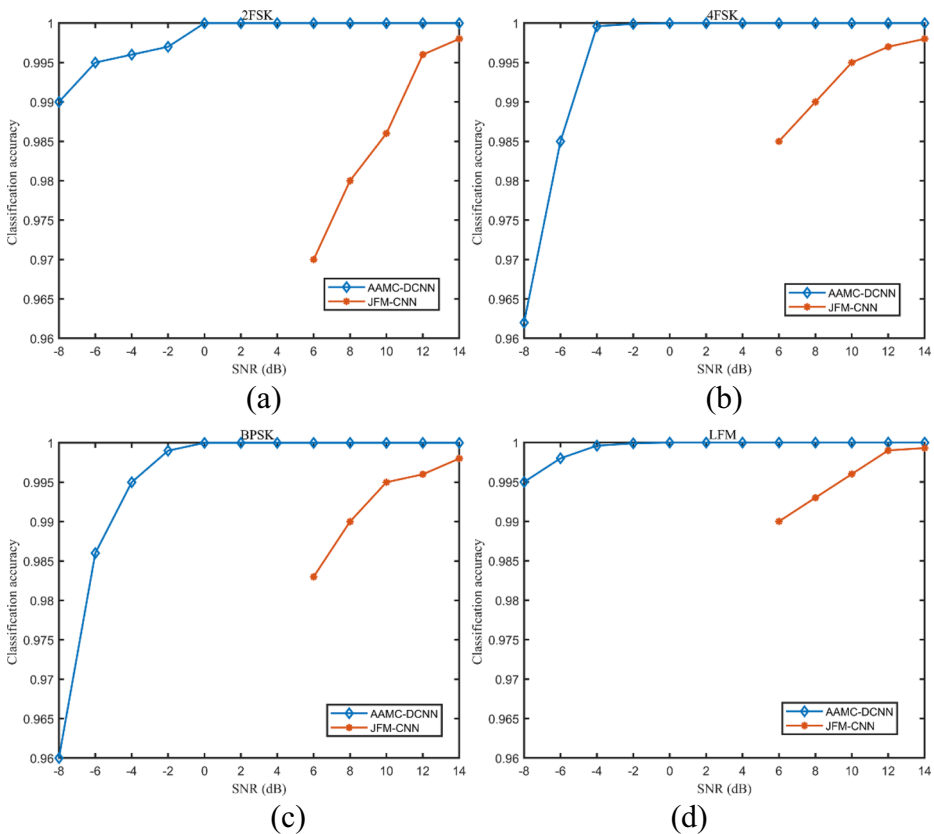
Fig. 7 The classification performance of four modulation types versus SNR in AAMC-DCNN and JFM-CNN

6 Conclusions

This paper presented an accurate automatic modulation classification algorithm based on dense convolutional neural networks, aiming to improve the recognition accuracy at the lower SNR environment. The proposed algorithm framework owns a more radical dense-connection mechanism compared with DenseNet and connects each layer to every other layer in a feed-forward pattern. The algorithm owns the competitive advantages of strengthening the feature reuse and extracting the detailed feature, for improving the recognition performance of radar waveform at the lower SNR. It was worth mentioning that the classification accuracy can be up to 93.4% when the SNR is −8 dB, and even reach to 100% at 0 dB, which demonstrated the superior performance over others, especially at the lower SNR. The confusion matrices demonstrated that the classification accuracies of LFM and SFM possessed the best performance over other modulation types. The present work provided an effective experimental foundation for the research of recognizing the radar signal waveform.

References

1. Ayazgok S, Erdem C, Ozturk MT, Orduyilmaz A, Serin M (2018) Automatic antenna scan type classification for next-generation electronic warfare receivers. IET Radar Sonar Navig 12(4):466–474. https://doi.org/10.1049/iet-rsn.2017.0354
2. Cao R, Cao JW, Mei JP, Yin C, Huang XG (2019) Radar emitter identification with bispectrum and hierarchical extreme learning machine. Multimed Tools Appl 78(20):28953–28970. https://doi.org/10.1007/s11042-018-6134-y
3. Chen H, Yin JJ, Yeh CM, Lu YB, Yang JY (2020) Inverse synthetic aperture radar imaging based on time-frequency analysis through neural network. J Electron Imaging 29(1):20. https://doi.org/10.1117/1.jei.29.1.013003
4. Gao J, Shen L, Gao L, Lu Y (2019) A rapid accurate recognition system for radar emitter signals. Electronics 8(4):463. https://doi.org/10.3390/electronics8040463
5. Glorot X, Bordes A, Bengio Y (2011) Deep sparse rectifier neural networks. In: Int. conf. on artificial intelligence and statistics, Fort Lauderdale, USA. pp. 315–323
6. Guo Q, Yu X, Ruan G (2019) LPI radar waveform recognition based on deep convolutional neural network transfer learning. Symmetry-Basel 11(4):540. https://doi.org/10.3390/sym11040540
7. He K, Zhang X, Ren S, Sun J (2016) Deep residual learning for image recognition. In: computer vision and pattern recognition, Nevada, USA. pp. 770–778
8. Huang G, Liu Z, Van Der Maaten L, Weinberger KQ (2017) Densely connected convolutional networks. In: IEEE conf. on computer vision and pattern recognition, Honolulu, USA, pp. 4700–4708
9. Huang Z, Ma Z, Huang G (2019) Radar waveform recognition based on multiple autocorrelation images. IEEE Access 7:98653–98668. https://doi.org/10.1109/access.2019.2930250
10. Ioffe S, Szegedy CJapa (2015) Batch normalization: Accelerating deep network training by reducing internal covariate shift. In: Int. Conf. on Machine Learning, Lille, France. pp. 1–11
11. Key ELJIA, Magazine ES (2004) Detecting and classifying low probability of intercept radar [book review]. IEEE Aerosp Electron Syst Mag 19(6):39–41. https://doi.org/10.1109/MAES.2004.1308837
12. Kingma DP, Ba J Adam (2015): A method for stochastic optimization. In: Int. Conf. for Learning Representations, San Diego, USA. pp. 1–15
13. Kishore TR, Rao KD (2017) Automatic intrapulse modulation classification of advanced LPI radar waveforms. IEEE Trans Aerosp Electron Syst 53(2):901–914. https://doi.org/10.1109/taes.2017.2667142

14. Kong S-H, Kim M, Linh Manh H, Kim E (2018) Automatic LPI radar wave form recognition using CNN. IEEE Access 6:4207–4219. https://doi.org/10.1109/access.2017.2788942
15. Linh Manh H, Kim M, Kong S-H (2019) Automatic recognition of general LPI radar waveform using SSD and supplementary classifier. IEEE Trans Signal Process 67(13):3516–3530. https://doi.org/10.1109/tsp.2019.2918983
16. Liu Z-M, Yu PS (2019) Classification, denoising, and deinterleaving of pulse streams with recurrent neural networks. IEEE Trans Aeros Electron Syst 55(4):1624–1639. https://doi.org/10.1109/taes.2018.2874139
17. Liu Y, Xiao P, Wu H, Xiao W (2015) LPI radar signal detection based on radial integration of Choi-Williams time-frequency image. J Sys Eng Electron 26(5):973–981
18. Lu X, Ma C, Ni B, Yang X, Reid I, Yang M (2018) Deep regression tracking with shrinkage loss. In: 15th European conference on computer vision, Munich, Germany. pp. 369–386
19. Lu X, Wang W, Ma C, Shen J, Shao L, Porikli F (2019) See more, know more: unsupervised video object segmentation with co-attention siamese networks. In: computer vision and pattern recognition, Long Beach, USA. pp. 3623–3632
20. Lundén J, Koivunen V (2007) Automatic radar waveform recognition. IEEE J Sel Top Signal Process 1(1):124–136. https://doi.org/10.1109/jstsp.2007.897055
21. Ma Z, Huang Z, Lin A, Huang G (2019) Emitter signal waveform classification based on autocorrelation and time-frequency analysis. Electronics 8(12):1419. https://doi.org/10.3390/electronics8121419
22. Noor A, Zhao YQ, Khan R, Wu LW, Abdalla FYO (2020) Median filters combined with denoising convolutional neural network for Gaussian and impulse noises. Multimed Tools Appl 4:16–18568. https://doi.org/10.1007/s11042-020-08657-4
23. Pan SJ, Yang Q (2009) A survey on transfer learning. IEEE Trans Knowl Data Eng 22(10):1345–1359. https://doi.org/10.1109/TKDE.2009.191
24. Qin Z, Zhou X, Zhang L, Gao Y, Liang Y-C, Li GY (2019) 20 years of evolution from cognitive to intelligent communications. IEEE Trans Cognitive Commun Netw 6(1):6–20. https://doi.org/10.1109/TCCN.2019.2949279
25. Simonyan K, Zisserman A (2014) Very deep convolutional networks for large-scale image recognition. In: computer vision and pattern recognition, Columbus, USA. pp. 1–14
26. Srivastava RK, Greff K, Schmidhuber J (2015) Training very deep networks. In: 28th international conference on neural information processing systems, Montrea, Canada. pp. 2377–2385
27. Wan J, Yu X, Guo Q (2019) LPI radar waveform recognition based on CNN and TPOT. Symmetry-Basel 11(5):725. https://doi.org/10.3390/sym11050725
28. Wang C, Wang J, Zhang X (2017) Automatic radar waveform recognition based on time-frequency analysis and convolutional neural network. In: IEEE Int. Conf. on Acoustics, Speech and Signal Processing, New Orleans, USA, March 2017. IEEE, new Orleans, USA, pp 2437–2441
29. Wang W, Lu X, Shen J, Crandall DJ, Shao L (2019) Zero-shot video object segmentation via attentive graph neural networks. In: international conference on computer vision, Seoul, Korea. pp. 9236–9245
30. Wang Q, Du P, Yang J, Wang G, Lei J, Hou C (2019) Transferred deep learning based waveform recognition for cognitive passive radar. Signal Process 155:259–267. https://doi.org/10.1016/j.sigpro.2018.09.038
31. Wang F, Yang C, Huang S, Wang H (2019) Automatic modulation classification based on joint feature map and convolutional neural network. IET Radar Sonar Navig 13(6):998–1003. https://doi.org/10.1049/iet-rsn.2018.5549
32. Wang Q, Du P, Liu X, Yang J, Wang G (2020) Adversarial unsupervised domain adaptation for cross scenario waveform recognition. Signal Process 171:107526. https://doi.org/10.1016/j.sigpro.2020.107526
33. Wei SJ, Qu QZ, Su H, Wang M, Shi J, Hao XJ (2020) Intra-pulse modulation radar signal recognition based on CLDN network. Iet Radar Sonar And Navigation 14(6):803–810. https://doi.org/10.1049/iet-rsn.2019.0436
34. Wu Z, Zhou S, Yin Z, Ma B, Yang Z (2017) Robust automatic modulation classification under varying noise conditions. IEEE Access 5:19733–19741. https://doi.org/10.1109/ACCESS.2017.2746140
35. Zhang M, Diao M, Gao L, Liu L (2017) Neural networks for radar waveform recognition. Symmetry-Basel 9(5):75. https://doi.org/10.3390/sym9050075
36. Zhang M, Diao M, Guo L (2017) Convolutional neural networks for automatic cognitive radio waveform recognition. IEEE Access 5:11074–11082. https://doi.org/10.1109/access.2017.2716191
37. Zhang J, Li Y, Yin J (2018) Modulation classification method for frequency modulation signals based on the time-frequency distribution and CNN. IET Radar Sonar Navig 12(2):244–249. https://doi.org/10.1049/iet-rsn.2017.0265
38. Zhang Z, Wang C, Gan C, Sun S, Wang M (2019) Automatic modulation classification using convolutional neural network with features fusion of SPWVD and BJD. IEEE Trans Signal Infor Process Net 5(3):469–478. https://doi.org/10.1109/tsipn.2019.2900201

39. Zhou R, Liu F, Gravelle CW (2020) Deep learning for modulation recognition: a survey with a demonstration. IEEE Access 8(99):67366–67376. https://doi.org/10.1109/ACCESS.2020.2986330
40. Zhu M, Li Y, Pan Z, Yang J (2020) Automatic modulation recognition of compound signals using a deep multi-label classifier: a case study with radar jamming signals. Signal Process 169:107393. https://doi.org/10.1016/j.sigpro.2019.107393
41. Zorzi S, Maset E, Fusiello A, Crosilla F (2019) Full-waveform airborne LiDAR data classification using convolutional neural networks. IEEE Trans Geosci Remote Sensing 57(10):8255–8261. https://doi.org/10.1109/tgrs.2019.2919472

Publisher's note   Springer Nature remains neutral with regard to jurisdictional claims in published maps and institutional affiliations.

Weijian Si is currently a Professor at Harbin Engineering University. He received the B.E degree from Beihang University, in 1994, and the Ph.D. degree from Harbin Engineering University, in 2004. From 1995 to 1999, he joined the 35th Institute of China Aerospace Science and Industry Corporation, where he was engaged in scientific research on radar signal processing. His main research interests include radar signal detection, processing and classification, high precision passive direction finding, and spatial spectrum estimation.

Chenxia Wan is currently Ph.D student at Harbin Engineering University. She received the B.E degree from Henan Agricultural University Henan, in 2016, and the M.S. degree from Henan University of Technology, in 2019. Her research interests include radar signal processing, radar waveform classification, and deep learning.

Chunjie Zhang is currently an Associate Professor at Harbin Engineering University. She received the B.E. and Ph.D. degrees from Harbin Engineering University, in 2004 and 2006, respectively. Her main research interests include wideband channelized receiver, pulse compression signal processing, and microwave spectrum analysis based on the photonic signal processing.